DNA sequencing by denaturation: experimental proof of concept with an integrated fluidic device

Ying-Ja Chen, Eric E. Roller and Xiaohua Huang*

Received 16th October 2009, Accepted 8th January 2010
First published as an Advance Article on the web 9th February 2010
DOI: 10.1039/b921417h

We report the proof of concept of a novel DNA sequencing technology called sequencing by denaturation (SBD). SBD is based on the Sanger sequencing reaction performed on amplified target templates immobilized on a solid surface followed by the denaturation of these Sanger fragments. As these fluorescently labeled fragments denature sequentially, the fluorescence intensities in the four channels corresponding to the four base types are monitored in a flow cell. A sequencing instrument with a microfluidic flowcell has been custom-designed to integrate automated fluidics, temperature control, and fluorescence imaging. The denaturation profiles of several synthetic oligonucleotides were measured with this system and our data demonstrated the ability to sequence short DNA by SBD. SBD is a simple and fast method with the potential to improve the speed and cost of large-scale genome re-sequencing.

Introduction

Genome sequencing technology is important for many applications. For example, genome sequencing technologies can be applied to digital gene expression and epigenetic profiling on a genome scale.[1–5] It can also be used to sequence the genomes of many individuals and entire populations for the study of complex diseases such as cancer.[6,7] The field of genome science has been advancing greatly upon the availability of several next-generation DNA sequencing platforms.[8–14] These platforms output orders of magnitude more DNA sequence data than traditional instruments. This is made possible by performing sequencing of short DNA strands on a solid surface to achieve high multiplexing capability. The sequencing chemistries developed to be compatible with the solid surface are different, but each chemistry sequences one to two bases at a time in many cycles, in which new batches of sequencing reagents containing polymerases and nucleotide analogs must be delivered. This contributes to the high cost of reagent supplies and long run time for every run with these next-generation sequencing instruments.

Here we present a sequencing strategy that can significantly reduce the cost of reagent supplies using a sequencing chemistry termed sequencing by denaturation (SBD). As described in our previous work on the principle and simulations of SBD,[15] DNA sequencing is performed on amplified templates separated spatially on a solid surface. First, a standard Sanger sequencing reaction is performed where fluorescently labeled dideoxynucleotides are randomly incorporated as the polymerase synthesizes the complementary strand from the amplified target template resulting in fragments of different lengths, each labeled with a fluorescent molecule corresponding to its ending base type.

Next, these fragments are denatured by heating, addition of chemical denaturants, or application of electric field. Because the melting temperature of a short DNA fragment is lower than a short DNA fragment with one additional base, the Sanger fragments are denatured sequentially from the shortest to the longest. By monitoring the decrease in fluorescence on the surface during this process, the signal can be analyzed to determine the base sequence of the target DNA template.

The theoretical basis of SBD has been established with a basic description of how DNA sequencing can be achieved experimentally.[15] Here we describe the construction of an integrated instrument system for DNA sequencing by SBD. We measured the denaturation profiles of oligonucleotides using the microfluidic system to demonstrate how sequencing can be performed. Finally, the performance of the system is analyzed and its utility is discussed.

Materials and methods

An integrated fluidic system for SBD

We have designed an integrated system to perform biochemical reactions and fluorescence detection on a single device. Fig. 1A shows a schematic of the system. It is based on an inverted fluorescent microscope (Zeiss Axiovert 200M) for fluorescence imaging. A custom-built reaction chamber is set on the stage of the microscope to hold a flow cell in place while allowing fluidic and temperature control over the flow cell. Detailed descriptions of each part are provided below.

Biochemical reaction chamber. Fig. 1B illustrates the design of the custom-made chamber. The assembled chamber and flow cell are shown in Fig. 1C and 1D, respectively. Biochemical reactions took place in a flow cell on a 75 mm × 50 mm × 170 μm cover slip. In each flow cell, there were three flow channels with dimensions of 5 mm × 62 mm defined by a piece of double-sided adhesive silicone tape (Scapa 702, ~120 μm thick) cut by a plot cutter (CraftROBO, Graphtech Inc.). The flow cell was covered with a glass slide with holes to allow reagents to flow through the

Department of Bioengineering, University of California, San Diego, 9500 Gilman Drive, La Jolla, CA 92093-0412, USA. E-mail: x2huang@ucsd.edu; Tel: +1 (858)822-2155

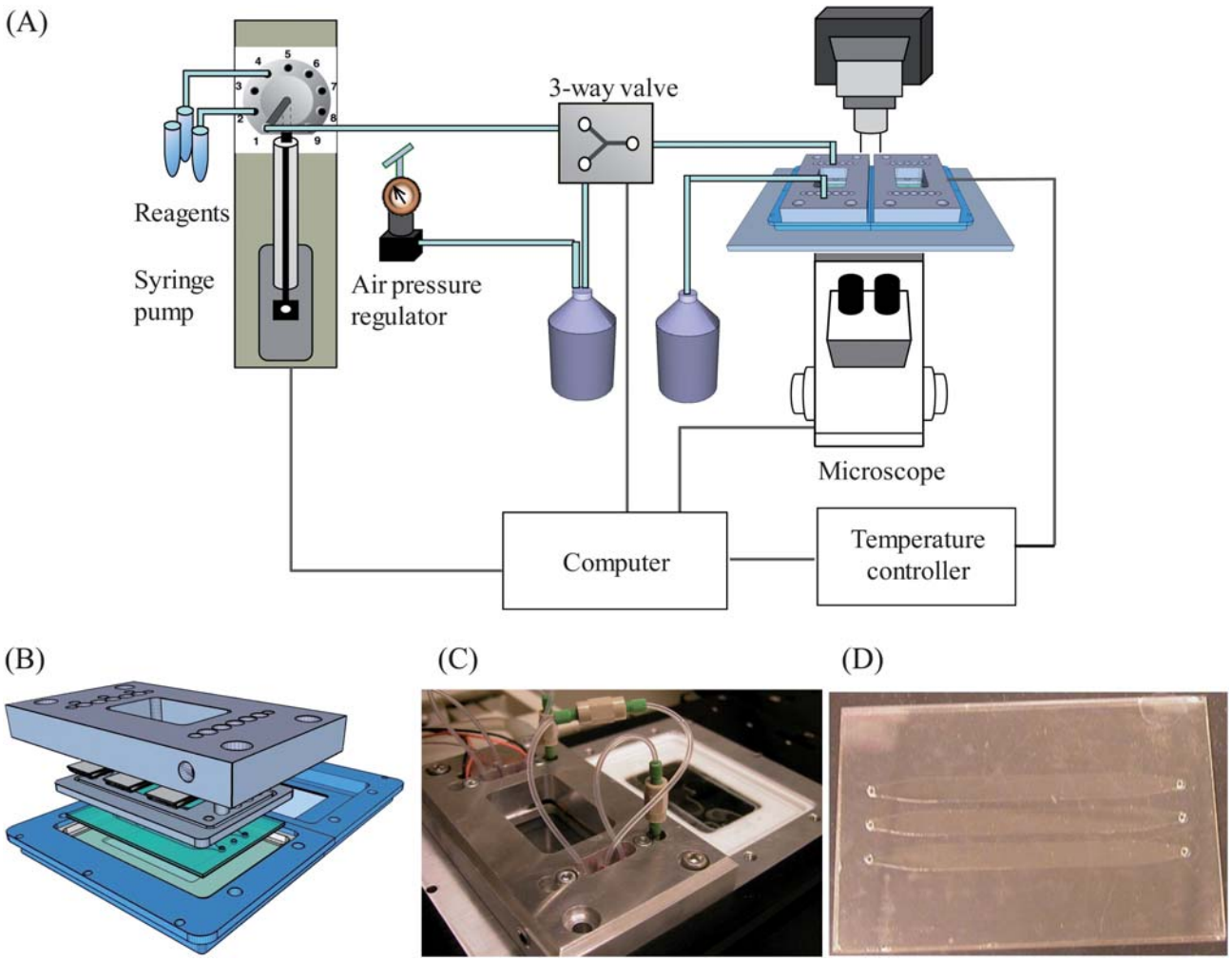

Fig. 1 An integrated system for DNA sequencing by denaturation. (A) A schematic of the system showing how the fluidic lines are connected to the reaction chamber where fluorescence imaging and temperature control take place. (B) The CAD drawing of the chamber illustrating the flow cell in the center with 3 pairs of thermoelectric modules for heating the chamber from above. The flow cell is sandwiched between a heat sink on the top and a microscope stage insert on the bottom. (C) A photograph of the chamber in its assembled form. (D) A photograph of the flow cell.

chamber. The fluidics were sealed by an o-ring to an aluminium plate, in which connections to the tubing were made with miniature connectors (Lee Minstac TMDA3207950Z). The temperature at the flow cell was controlled by thermoelectric modules on the top of the aluminium piece. On top of the thermoelectric modules was another aluminium block serving as the heat sink, whose temperature was held constant through an external water circulator (Julabo F25-HE). The bottom of the chamber was insulated from the microscope stage by a Teflon spacer.

Fluorescence imaging. The high-speed fluorescence imaging system consists of an inverted fluorescence microscope with motorized configuration (Zeiss Axiovert 200M), a high-speed 5-channel fast wavelength-switching light source (Lambda DG-5, Sutter Instruments), a motorized stage with linear encoders (BioPrecision 2, Ludl Electronic Products Ltd.), and an EMCCD camera with 1004 × 1002 pixels of 8 μm × 8 μm (iXon+ 885, Andor Technology PLC). A quadband-pass filter set (Pinkel set, FF01-440/521/607/700-25, Semrock Inc.) was used for three color imaging. The fluorescent channels were chosen by the excitation wavelength filtered by the DG-5 light switching device. Images were acquired using a plan-apochromat 20× objective with 0.8 NA in 50∼200 ms exposures with 5–50 EM gain on the CCD camera and 30%, 50%, or 100% of the output power from the light source to utilize the maximum dynamic range of the camera in every channel.

Temperature control. Four pairs of 8 W thermoelectric modules (MI1023T-02, Marlow Industries Inc.) were connected in parallel for temperature control. They were connected to a 13.8 V, 260 W power supply (RadioShack) and a temperature controller (TC-24-25, TE Technology) that was controlled by the computer automation program. The temperature controller maintained the temperature of the chamber at fixed temperatures using proportional-integral-derivative (PID) control or provided a fixed output voltage to the thermoelectric modules. A thermistor (MP-2379, TE Technology) was fixed to the aluminium plate near the flow cell to record the temperature in the chamber for feedback control. A linearly increasing temperature profile was established by providing a linearly increasing negative

output power through time. This nearly linear temperature profile was used during the measurement of the DNA denaturation profiles for sequencing.

Fluidics. Reagents were delivered to the flow cell through a syringe pump (Cavro XL3000, Tecan Systems). The wash buffer was flowed into the stainless steel tubing (1.6 mm OD, 0.75 mm ID, ~100 mm long) embedded into the aluminium block to preheat the solution before it entered the flow channel. Washing was driven by constant air pressure maintained through an air-pressure regulator and a miniature precision regulator (8812K31 and Airtrol R800-10, McMaster-Carr). The pressure-driven flow was used during denaturation detection to minimize inconsistent focus drift while imaging. A three-way solenoid valve (Lee LFHA1201160H) was used to switch between the syringe pump and the pressure-driven flow.

Measurements of denaturation profiles

Sample preparation. Glass cover slips were cleaned in 10% nitric acid for 30 min followed by washing with a large volume of 18.0 MΩ-cm deionized water and air dried after rinsing with acetone. They were then silanized with 2% 3-aminopropyl-triethoxysilane in 95% acetone (5% water) solution for 15 min. Then, they were washed 4 times in acetone, 3 min each, and cured at 110 °C for 30 min. Next, they were derivatized with 5 mM NHS-PEG_4-biotin (Product #21362, Pierce Biotechnology Inc.) in N,N-dimethylformamide containing 100 mM of triethylamine at room temperature for one hour and washed 4 times with acetone, 3 min each. Subsequently, the excess amino groups were blocked by acylation with 100 mM acetic anhydride in 1,4-dioxane with 100 mM triethylamine at room temperature for 30 min. After washing 4 times with acetone, 3 min each, and drying by blowing with filtered compressed air, the cover slips were stored under vacuum in a desiccator before being assembled into a flow cell for use.

Streptavidin-coated 1 μm superparamagnetic microbeads (Dynal MyOne-C1, Invitrogen Inc.) were immobilized onto the biotinylated cover slips by incubating them at 37 °C for 30 min in a 0.033 mg ml^{-1} solids suspension in 1X binding and washing buffer (B&W) which contains 1 M NaCl, 5 mM Tris-Cl, 1 mM EDTA, and 0.005% Triton X-100, pH 8.0. A permanent magnet was dragged transiently underneath the flow channel to pull the magnetic microbeads down to the biotinylated cover slip surface before and after the incubation. 200 nM of double-biotinylated oligonucleotides in 1X B&W buffer were incubated at 37 °C for 1 h to attach them to the microbeads as the target template for DNA sequencing. Under these concentrations, a saturating density of 0.8–1.4 × 10^6 template molecules per bead is estimated. Both steps were followed by washing with 2.5 ml of wash buffer containing 33 mM phosphate buffer, pH 7.2, and 0.05% Triton X-100.

Control beads were prepared by incubating 20 nM fluorescently labeled biotinylated oligonucleotides with 0.13 mg ml^{-1} microbeads in 1X B&W buffer at 37 °C 600 rpm on a thermal mixer for 1 h. These control beads were immobilized on the surface at 37 °C for 30 min followed by washing with 2.5 ml wash buffer. One set of images were acquired in this step for locating the control beads in the subsequent image analysis step. Next, 200 nM of fluorescently labeled oligonucleotides were hybridized to the templates attached to the microbeads in 1X B&W buffer at 37 °C for 1 h followed by washing with 2.5 ml wash buffer.

Measurement of individual denaturation curves. Six oligonucleotides, each differing in size by one base, were hybridized to the common target template one at a time in the conditions as described above to measure their individual denaturation curves. The sequences of the oligonucleotides are summarized in Table 1. Due to the limitation of our current imaging instrument, sequencing of only three different base types was performed. Three spectrally distinguishable Alexa dyes were chosen as labels. Alexa dyes were chosen for their photostability over temperature and continuous exposure, high quantum yield, and commercial availability for conjugation to oligonucleotides. The denaturation curves were measured by acquiring 200 images evenly while the temperature was increased from 35 °C to 80 °C with a slope of 0.33 °C min^{-1} by applying a linearly increasing output voltage from the thermoelectric module while the heat sink is held at a constant temperature of 20 °C. A fluid flow of 1.3 ml min^{-1} was applied by using 1.25 psi of air pressure during the entire denaturation experiment. Before each image was taken, an autofocus protocol was performed at a neighboring spot to ensure that the picture is in focus while avoiding photobleaching at the spots for image acquisition. The images were acquired at 50 ms exposure time, 30% output power from the DG5 light source, and 10 to 50 EM gain of the camera in order to achieve maximum dynamic range in each fluorescent channel without saturating the camera.

Measurement of denaturation profiles in three channels. The denaturation signals exhibited by the ensemble of 6 DNA fragments were measured in three fluorescent channels, each corresponding to one base in a single experiment. The 6 oligonucleotides were mixed in equal ratios at 33.3 nM each in 1X B&W buffer and hybridized to the common target template at 37 °C for 1 h. The denaturation profiles of 3 channels (Alexa488, Alexa546, and Alexa647) were measured simultaneously using the same protocol as described above by taking images at 200 evenly distributed temperature points ranging from 35 °C to 80 °C. In this case, the autofocus process was only performed in the 488 nm channel and three images were taken, one in each channel, before the stage was moved to the next position.

Image analysis. The images were analyzed using an ImageJ (NIH) plugin written in Java. The algorithm first subtracts the background using a rolling ball algorithm with a radius of 50 pixels. Then, the first image taken at the lowest temperature is thresholded to find the location of each bead using the Otsu algorithm.[16] For the subsequent images, a cross-correlation with the first image was computed to register the images before the same threshold image was used for analyzing the integrated intensity of the beads with sizes of 7–72 pixels. The intensities of the beads were saved as an array, which was later analyzed using a routine written in MATLAB to plot the denaturation curves. The average intensity of all the control beads, which appeared in the control image, was used as the maximum fluorescence level. The signal of each sample bead was divided by the average control intensity to adjust for photobleaching and the

Table 1 List of DNA sequences and melting temperatures. The bases where the template and the fluorescently labeled oligonucleotide probes hybridize to are underlined and the target region being sequenced is italicized

Oligonucleotide	Sequence	Melting temperature (T_m)		
		Predicted	Solution	Surface
Target template	5′-Biotin-TEG-(Biotin-TEG)-TACAGACTTAGTGGGGTAAAACTAGCA *TGACTGA*CTTCGTACATGACTGATGG TCGATAC-3′			
20merT_5Alx488	5′-Alexa488-CCATCAGTCATGTACGAAGT-3′	53.2	ND[a]	45.8
21merC_5Alx546	5′-Alexa546-CCATCAGTCATGTACGAAGTC-3′	55.1	54.1	48.0
22merA_5Alx647	5′-Alexa647-CCATCAGTCATGTACGAAGTCA-3′	57.3	54.3	49.8
24merT_5Alx488	5′-Alexa488-CCATCAGTCATGTACGAAGTCAGT-3′	60.5	56.9	53.0
25merC_5Alx546	5′-Alexa546-CCATCAGTCATGTACGAAGTCAGTC-3′	61.8	56.7	54.4
26merA_5Alx647	5′-Alexa647-CCATCAGTCATGTACGAAGTCAGTCA-3′	63.5	57.9	54.7
Alexa488 control	5′-Biotin-TEG-CCAT-(Biotin-TEG)-CAGTCATGTACGAAGTCAGT-Alexa488-3′			
Alexa546 control	5′-Biotin-TEG-CCAT-(Biotin-TEG)-CAGTCATGTACGAAGTC-Alexa546-3′			
Alexa647 control	5′-Biotin-TEG-CCAT-(Biotin-TEG)-CAGTCATGTACGAAGTCA-Alexa647-3′			

[a] Not determined.

temperature effect on the fluorescent efficiency. The adjusted signal was fit to a sigmoid function and normalized so that the denaturation signal dropped from 100% to 0%. For measurements where multiple oligonucleotides contribute to the same fluorescence channel, the negative derivative curve was taken and fit to the sum of Gaussian curves to resolve the individual components. Details of the data analysis process have been described previously.[15]

Results and discussion

Characterization of the integrated system

The integrated system was designed to combine fluorescence imaging with temperature and fluidic control for SBD. It allows for high-speed fluorescence imaging and scanning through a surface that is the size of a microscope slide while the temperature and fluid flow in the flow cell are controlled simultaneously in either an independent or synchronized fashion. A linearly increasing temperature profile with the desired ramping speed is established by controlling the initial value and slope of the output voltage to the thermoelectric modules. Before the system becomes fully functional, several issues must be considered. First, temperature increase causes thermal expansion of the device which results in a drift in the focus plane for imaging. This was characterized to be linearly related to the temperature and was corrected in the automation program. Second, the change in fluid flow rate perturbs the focus plane as well. This was avoided by applying a constant flow for the washing with an air pressure-driven flow held at constant air pressure from a large reservoir. Third, the fluorescent signal in SBD suffers from photobleaching due to extensive imaging and the fluorescence quantum yield of the organic dyes decreases at higher temperatures. Exposure times were kept at the minimal level to alleviate this issue. In addition, an internal control containing only the fluorescent molecules directly immobilized onto the surface or microbead was included in the experiments so that these effects can be corrected for in the analysis.

Measurement of individual denaturation curves

SBD determines the base sequence of DNA by distinguishing the melting points of short DNA fragments. Therefore, in order to determine the feasibility of SBD, we must be able to measure and distinguish the difference in melting points of short DNA fragments with single-base resolution. We measured the denaturation curves of 6 individual DNA fragments with lengths from 20 to 26, excluding length 23, on the surface in the device. Their sequences are summarized in Table 1. Each shorter fragment is a substring of the longer fragments. Three different fluorescent molecules are selected by their brightness, spatial separation from each other, and the availability of filter sets for imaging. Each fluorescently labeled DNA fragment was hybridized to a common template that was immobilized on the microbeads on the surface. As the temperature increases, the fluorescent intensity on the surface was detected to measure the fraction of DNA fragments that remained in double-stranded form. The fluorescent signals of the sample beads were normalized with fluorescent signals of the control beads, on which fluorescently labeled DNA strands were immobilized directly.

The melting properties of oligonucleotides are controlled by several factors. First, the oligonucleotide concentration affects the melting temperature unless the melting curve is a two-state cooperative transition that exhibits either all hybridized or all denatured states. Typical thermodynamic parameters were established for oligonucleotide concentrations ranging from 50 nM to 100 μM. The oligonucleotide concentration used in the current study is 200 nM during incubation for both attachment of target template and hybridization of the reporter probes.

Second, the concentration of monovalent salt is positively correlated to the melting temperature of oligonucleotides. Here a fixed concentration of 33 mM phosphate buffer equivalent to 49 mM monovalent salt is used in the wash buffer in order to maintain constant ionic strength while denatured oligonucleotide fragments were washed away. By washing away denatured fragments, the denaturation process is driven away from equilibrium. This process not only removes background fluorescence from the surface, but also facilitates the detection of a more defined transition without the complications from equilibrium re-hybridization.

Fig. 2A shows the average signal from hundreds of microbeads for each oligonucleotide fragment. As shown in the figure, the melting temperature of the fragments increases monotonically as the length of the fragment increases. Fig. 2B shows the negative derivatives of these curves. The peaks indicate the transition points of the denaturation process of each oligonucleotide fragment, which is positively correlated to the melting temperature. Table 1 shows the predicted melting temperatures and the melting temperatures measured in solution[15] and on the surface. The melting temperatures measured on the surface are lower than those measured in solution. This may be due to the way the temperature was measured in our device where the thermistor is placed at the end of the device while the fluid flows through the stainless steel tubing embedded directly underneath the thermoelectric modules, thereby giving a different temperature reading than the actual temperature at the sample. Nevertheless, a similar trend in the two measurement systems indicates that the denaturation profiles measured on the surface can be analyzed through the same algorithm as presented previously to decode the base sequence of DNA.

Another factor to consider in these measurements is the potential detachment of target templates from the surface by heating and washing during detection. In order to prevent target templates from detaching from the microbeads, templates were labeled with two biotin moieties. Even if one biotin dissociates from the streptavidin on the microbead, the other biotin may remain bound. Given the binding strength of biotin and streptavidin at the measured conditions, a very low percentage of templates will dissociate and be washed away. In addition, control beads in these measurements can be used not only to correct for the fluorescence decrease due to photobleaching and temperature effect, but also to correct for the detachment of target templates during detection since the fluorescent probes on the control beads may detach from the beads in the same manner.

In Fig. 2A, the denaturation curves are flat before and after the denaturation event. Although control beads were used to correct for photobleaching, fluorescent molecules with spectra towards the longer wavelengths have lower signal strengths and show a characteristic decrease in the melting curve before the transition and a slight increase in the melting curve after the transition. This could be an inherent property of the denaturation process on the surface. Since the denaturation process is driven away from equilibrium, there is less observed cooperativity. This may also explain why the denaturation curves measured on the surface are not as sharp as those measured in solution.

Measurement of denaturation profiles in three channels

The signal from SBD is measured in three fluorescence channels. In each channel, the fluorescence signal is the sum of the contribution of each DNA fragment labeled with the fluorescent molecule corresponding to the type of the terminal base. We have measured the three-channel fluorescence signals from 6 oligonucleotide fragments that were hybridized to one common template. In each channel, two oligonucleotide probes contribute to its signal, the 20-mer and 24-mer for T, 21-mer and 25-mer for C, and 22-mer and 26-mer for A.

Fig. 3A shows the signal measured in the three channels. It can be seen that each channel corresponds to two transitions contributed by the two fragments. This data was analyzed using

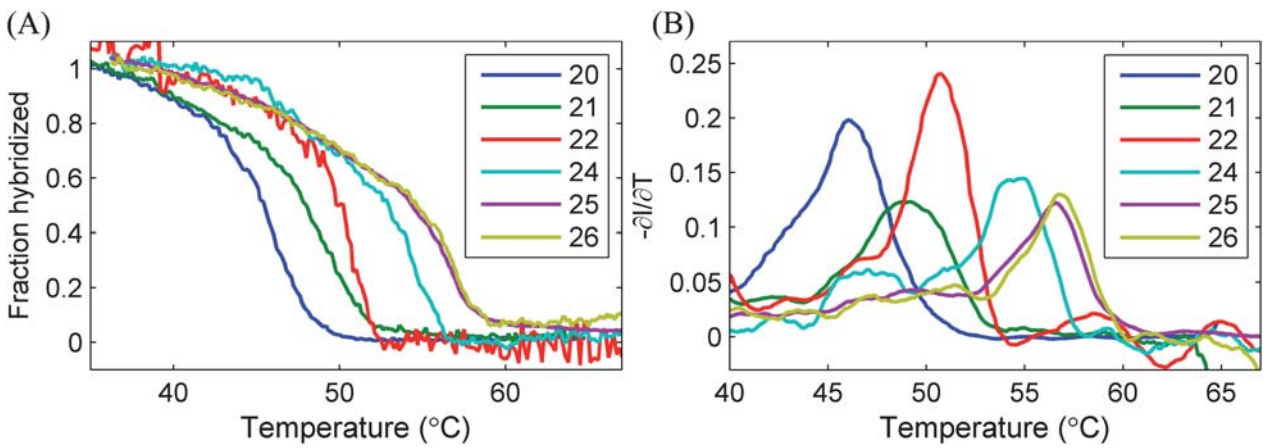

Fig. 2 The denaturation curves of six oligonucleotide probes. (A) The denaturation curves of six oligonucleotides were measured on the surface. The melting temperatures (transition points) of the DNA fragments increase as the length of the fragment increases. (B) The negative derivatives of the measured denaturation curves. The transition points are clearly separated by reading from the positions of the peaks.

an algorithm we developed previously.[15] In Fig. 3B the negative derivatives of the fluorescent signals are shown. Each of the curves is fit to the sum of two Gaussian curves to determine the components contributing to the fluorescence signal. Fig. 3C shows that the fit overlaps with the original signal well, indicating a good fit. In Fig. 3D, the component curves determined by the fit are plotted. The base sequence of the template DNA is determined from the order of the peaks and yields the correct sequence: TCA(G)TCA. Due to technical challenges of four-color imaging, the fluorescence channel corresponding to "G" was not measured in this experiment. A fourth fluorescence channel with a bright fluorescence signal and little photobleaching is required. A better fluorescence detection system will also improve our ability to distinguish one melting curve from another. However, these results demonstrate that the denaturation profiles of DNA fragments can be measured on the surface in a device and this property can be used to decode the base sequence of DNA.

Advantages and limitations of SBD

The system was designed with a potential application in genome sequencing in mind. The speed of genome sequencing on this system is limited by the imaging speed. Therefore, for the optimization of speed, high-speed and high-sensitivity imaging components were chosen to minimize scanning and exposure times.

The throughput of the system depends on the number of features detected within each image. In SBD, the target templates are immobilized and detected on the surface. In the current study, target templates were separated spatially by attaching them on different microbeads immobilized on the surface. The imaging throughput was limited by the separation of the randomly distributed microbeads. However, SBD is compatible with array technologies[17,18] that can be used to pack the templates in very high-density with each template on an area as small as 1 μm^2. This will allow more efficient imaging to be performed.

The throughput for SBD also depends on the number of images required per base sequenced. This depends on the number of sampling points required during the temperature increase in order to accurately account for the denaturation profile and the read length. We estimate that the read length of the system will be around 20 bases. By taking 100 data points with 0.5 °C difference between each sampling while the temperature is increased from 25 to 75 °C, then 5 images are taken per base sequenced. These parameters determine the limitations of the throughput of SBD. It is comparable to other next-generation sequencing platforms.

Another important factor to consider for genome sequencing is cost. In SBD, the major cost for sequencing comes from the cost of polymerase and labeled nucleotides during the Sanger

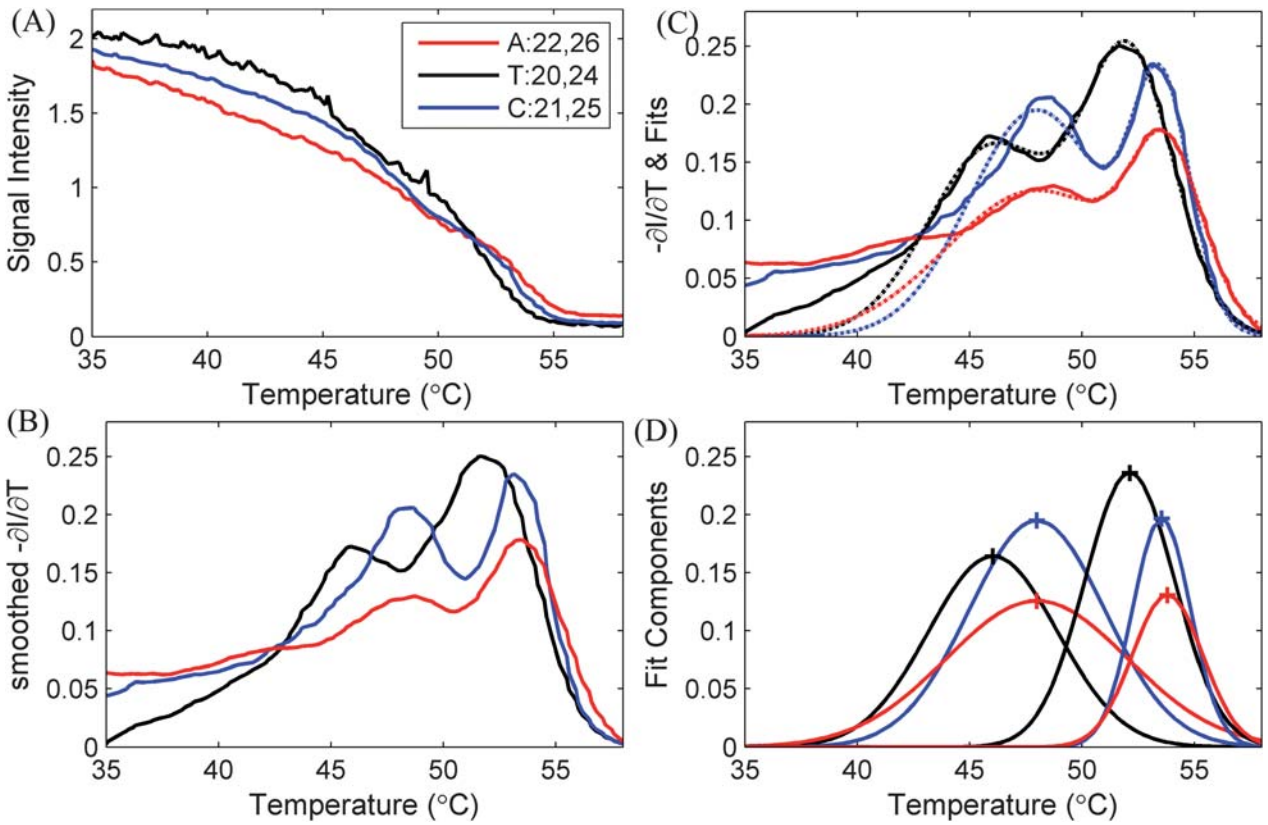

Fig. 3 The denaturation profiles in three channels mimicking the sequencing of 6 bases. (A) The fluorescent signals were measured in three channels. (B) The negative derivatives of the fluorescence signals were taken. (C) The fit of the negative derivatives overlaps with the negative derivatives well. (D) By the order of the peaks of the component curves of the fit, the base sequence of the template DNA can be determined correctly. The peak positions are 46.0, 48.0, 48.0, 52.1, 53.5, 53.8 °C, respectively.

sequencing reaction. Fortunately, this reaction only needs to be performed once in the entire sequencing run as opposed to once per cycle in the cyclic sequencing chemistries. Moreover, because SBD chemistry is compatible with array technologies that can be used to pack the target templates in very high densities, a minimal volume of reagents can be used. In our current flow cell design, about 150 μl of solution is required for the entire sequencing reaction. This is a dramatic improvement over currently available next-generation sequencing technologies since only a very small volume of reagent is required for the entire sequencing run. Similarly, the cost of preparing the genomic library of templates can be kept low if small microbeads are used and the volume of solution for creating emulsions for single molecule DNA amplification is small. Therefore, SBD with our system could potentially be used for high-throughput genome re-sequencing at a very low cost because of the simple sequencing chemistry inherent in the technology.

SBD technology has a limited read length due to an inability to separate the melting temperatures as the read lengthens. However, these short-read sequences are still useful for many applications. For instance, a 9-base tag can uniquely determine the identity of an mRNA if the tag is isolated from a defined position.[19] Therefore, with an estimated read length of 20, SBD can be useful for digital gene expression profiling.

Conclusions

We have designed and fabricated a device with integrated temperature, fluidic control, and fluorescence imaging for sequencing application. It has the capability for performing high-speed fluorescence imaging while biochemical reactions with precisely controlled temperature profiles take place. It has been used to measure the fluorescent signal of the SBD process. The denaturation profiles of 6 DNA fragments hybridized to a common target template was measured and analyzed to determine the base sequence of the template. The correct sequence was determined. This demonstrated the feasibility of SBD. However, further experiments will be required to demonstrate the full potential of SBD.

Based on the standard Sanger sequencing chemistry and simple denaturation of DNA, SBD has the advantage of simplicity and low cost since the sequencing reaction is only performed once in a small volume. However, due to the small differences between the melting temperatures of DNA fragments, the read length of SBD is expected to be limited, perhaps as long as 20 bases in a single run. SBD also has a high demand on imaging. Despite these limitations, we believe that SBD offers great reduction in genome sequence cost that can be combined with other methods to achieve higher-throughput and lower-cost genome sequencing.

Acknowledgements

This work was supported in part by grants from the NIH/NHGRI (R21HG003587, R21HG004130 and 1R01HG005096) and the NSF under a CAREER award to X. H. (BES-0547193).

References

1 M. P. Ball, J. B. Li, Y. Gao, J.-H. Lee, E. M. LeProust and I.-H. Park, *et al.*, *Nat. Biotechnol.*, 2009, **27**, 361–368.
2 S. J. Cokus, S. Feng, X. Zhang, Z. Chen, B. Merriman and C. D. Haudenschild, *et al.*, *Nature*, 2008, **452**, 215–219.
3 J. Deng, R. Shoemaker, B. Xie, A. Gore, E. M. LeProust and J. Antosiewicz-Bourget, *et al.*, *Nat. Biotechnol.*, 2009, **27**, 353–360.
4 J. B. Kim, G. J. Porreca, L. Song, S. C. Greenway, J. M. Gorham and G. M. Church, *et al.*, *Science*, 2007, **316**, 1481–1484.
5 K. Zhang, J. B. Li, Y. Gao, D. Egli, B. Xie and J. Deng, *et al.*, *Nat. Methods*, 2009, **6**, 613–618.
6 F. Dahl, J. Stenberg, S. Fredriksson, K. Welch, M. Zhang and M. Nilsson, *et al.*, *Proc. Natl. Acad. Sci. U. S. A.*, 2007, **104**, 9387–9392.
7 T. J. Ley, E. R. Mardis, L. Ding, B. Fulton, M. D. McLellan and K. Chen, *et al.*, *Nature*, 2008, **456**, 66–72.
8 W. J. Ansorge, *New Biotechnol.*, 2009, **25**, 195–203.
9 D. R. Bentley, S. Balasubramanian, H. P. Swerdlow, G. P. Smith, J. Milton and C. G. Brown, *et al.*, *Nature*, 2008, **456**, 53–59.
10 T. D. Harris, P. R. Buzby, H. Babcock, E. Beer, J. Bowers and I. Braslavsky, *et al.*, *Science*, 2008, **320**, 106–109.
11 R. A. Holt and S. J. M. Jones, *Genome Res.*, 2008, **18**, 839–846.
12 E. R. Mardis, *Trends Genet.*, 2008, **24**, 133–141.
13 M. Margulies, M. Egholm, W. E. Altman, S. Attiya, J. S. Bader and L. A. Bemben, *et al.*, *Nature*, 2005, **437**, 376–380.
14 J. Shendure, G. J. Porreca, N. B. Reppas, X. Lin, J. P. McCutcheon and A. M. Rosenbaum, *et al.*, *Science*, 2005, **309**, 1728–1732.
15 Y.-J. Chen and X. Huang, *Anal. Biochem.*, 2009, **384**, 170–179.
16 N. Otsu, *IEEE Trans. Systems Man Cybernetics*, 1979, **SMC-9**, 62–66.
17 K. D. Barbee and X. Huang, *Anal. Chem.*, 2008, **80**, 2149–2154.
18 K. D. Barbee, A. P. Hsiao, M. J. Heller and X. Huang, *Lab Chip*, 2009, **9**, 3268–3274.
19 V. E. Velculescu, L. Zhang, B. Vogelstein and K. W. Kinzler, *Science*, 1995, **270**, 484–487.